ACS APPLIED MATERIALS & INTERFACES

Research Article

www.acsami.org

Benzodipyrrolidone (BDP)-Based Polymer Semiconductors Containing a Series of Chalcogen Atoms: Comprehensive Investigation of the Effect of Heteroaromatic Blocks on Intrinsic Semiconducting Properties

Kyu Cheol Lee,[†,§] Won-Tae Park,[‡,§] Yong-Young Noh,[*,‡] and Changduk Yang[*,†]

[†]School of Energy and Chemical Engineering, KIER-UNIST Advanced Center for Energy, Low Dimensional Carbon Materials Center, Ulsan National Institute of Science and Technology (UNIST), Banyeon-ri 100, Eonyang-eup, Ulju-gun, Ulsan, 689-798 South Gyeongsang, South Korea

[‡]Department of Energy and Materials Engineering, Dongguk University, 26 Pil-dong, 3 ga, Jung-gu, Seoul 100-715, South Korea

Supporting Information

ABSTRACT: In order to determine the effects of actual 'chalcogen atoms' on semiconducting properties for application in a variety of optoelectronic devices, a class of donor (D)−acceptor (A) polymer semiconductors, namely **PBDP-Fu**, **PBDP-Th**, and **PBDP-Se**, containing the recently formulated benzodipyrrolidone (BDP) accepting unit and furan (Fu), thiophene (Th), or selenophene (Se) as a donating unit has been synthesized, characterized, and used in an active layer of organic field-effect transistors (OFETs). With the LUMO levels being comparatively consistent for all three polymers (−3.58 to −3.60 eV) due to the dominant BDP contribution to the polymer backbone, the HOMO energies are somewhat sensitive to the structurally distinctive feature of the donor counits used. Utilizing a combination of X-ray diffraction (XRD) and atomic force microscopy (AFM), it is apparent that further crystalline domains occur with edge-on orientation for the polymers (**PBDP-Th** and **PBDP-Se**) with relatively heavier chalcogen atoms such as Th and Se, compared with **PBDP-Fu** which has a rather amorphous nature. Investigation of their OFET performance indicates that all the polymers show well balanced ambipolar operations. The desirable morphological structures of both the **PBDP-Th** and **PBDP-Se** result in higher mobilities in OFETs than those of **PBDP-Fu**. In particular, 200 °C annealed PBDP-Se OFETs results in ambipolarity being mobile for both holes of up to 1.7×10^{-2} cm^2/V·s and electrodes of up to 1.9×10^{-2} cm^2/V·s. In addition, OFETs with **PBDP-Th** show nearly equivalent charge carrier mobilities for both holes ($\mu_h = 1.2 \times 10^{-2}$ cm^2/V·s) and electrons ($\mu_e = 1.1 \times 10^{-2}$ cm^2/V·s). Consequently, we systematically demonstrate how the manipulation of existing heteroaromatics can modulate the electronic properties of conjugated D−A polymers, elucidating structure−property relationships that are desirable for the rational design of next generation materials.

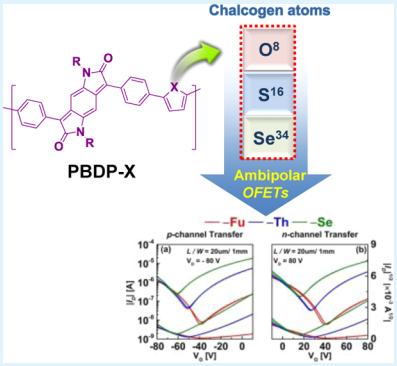

KEYWORDS: *ambipolar semiconductors, benzodipyrrolidone, chalcogen atoms, heteroaromatics, organic field-effect transistors, semiconductors*

1. INTRODUCTION

π-Conjugated polymer semiconductors are expected to be one of the promising key elements[1−3] for innovative display technologies,[4−8] because, in spite of their current poor stability, they have many advantages over silicon-based semiconductor materials, including flexibility, lightweight, ultralow-cost, and processability. Special attention has been paid to the design of conjugated donor (D)−acceptor (A) polymers, since this approach can enhance the intermolecular and intramolecular interactions which directly govern the molecular ordering and $\pi-\pi$ stacking of the polymer chains in the solid state, thus boosting the effective charge transport efficiency.[9] In addition, D−A polymers enable the realization of large area integrated circuits (ICs) based on complementary inverters and light emitting transistors (LETs) by a simple blanket coating without the sophisticated patterning processes of the organic semiconducting layer since the polymers can have both electron and hole transport in one polymer chain.[10,11] To achieve high performance ambipolar ICs and LETs, high and well-balanced electron and hole mobility is required.[12]

In recent years, bislactam-based chromophores such as diketopyrrolopyrrole (DPP),[13−18] benzodipyrrolidone (BDP),[19−22] isoindigo (IIG),[23−28] and thienoisoindigo (TIIG)[29−33] (Figure 1), so-called 'high-performance pigments', have been the most frequently used electron-accepting building blocks for constructing D−A type polymers with high charge

Received: December 21, 2013
Accepted: March 12, 2014
Published: March 12, 2014

   dx.doi.org/10.1021/am405917a | ACS Appl. Mater. Interfaces 2014, 6, 4872−4882

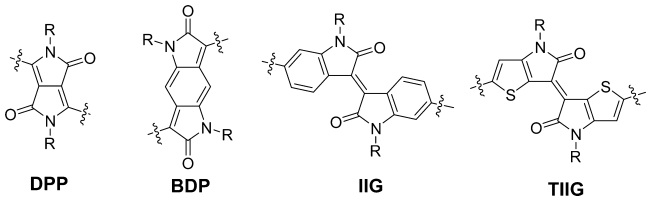

Figure 1. Structures of diketopyrrolopyrrole (DPP), benzodipyrrolidone (BDP), isoindigo (IIG), and thienoisoindigo (TIIG).

carrier mobility. In line with the consideration of an effective D−A strategy, various thiophene-based moieties as the natural choice for electron-donating units within the main backbone have been ubiquitously incorporated into bislactam-containing D−A polymers for applications in organic field-effect transistors (OFETs).[34]

In order to maximize the charge transport caused by effective overlap integrals of wave functions between neighboring molecules, our group and several other groups recently developed selenophene-comprising D−A polymers based on a bislactam core having higher charge-transport performances.[35−39]

At the same time, a growing interest in oligofurans as an alternative to other heteroaromatics used has developed since it is believed they can be obtained from biomass and are considered 'green' electronic materials;[40,41] they also have similar energy levels and a comparable degree of aromaticity relative to thiophene counterparts.[42,43] Despite the fact that furans are smaller overlap integrals and have lower polarizabilities than thiophenes,[44−46] recent progress in the development of bislactam-based D−A polymers containing furan for OFETs has yielded materials with high charge carrier mobilities comparable with those obtained for their thiophene analogues.[47−49] However, systematic investigations of heteroaromatics-comprising D−A polymers with different aromaticities have not yet been subjected to the same bislactam framework, and their own unique advantages as aforementioned have been enjoyed within the different acceptor building blocks. For example, the analogues of DPP-benzothiadiazole polymer (PDPP-BT), in which the neighboring thiophene units on DPP core are replaced with either thiophene (Th) or selenophene (Se), were developed by Heeney and Sirringhaus et al. Besides, Sonar, Li, and Dodabalapur et al. reported the synthesis of BT-based polymer comprised of furan (Fu)-substituted DPP combined with BT and its use in OFETs.[50] A series of publications based on the molecules of varying chalcogen atoms in different research groups followed,[51−56] shedding light on their interesting properties.

From our attempt to uncover the actual 'chalcogen atom' impact on intrinsic polymer properties, we selected the recently conceived benzodipyrrolidone (BDP) accepting moiety that is described as an elongated DPP structure. Herein, we report the synthesis of a series of BDP-based D−A polymers, **PBDP-Fu**, **PBDP-Th**, and **PBDP-Se**, by polymerizing donor moieties, Fu, Th, and Se, with the soluble BDP acceptor unit. Other comparative studies of these polymers also represent a step toward a structure−property relationship regarding the chalcogen atoms as the counterpart comonomers for OFETs based on bislactam structures. We believe that these cogent studies, relating to energy levels, morphology, molecular packing, and carrier transport as a function of heteroaromatic building blocks, are extremely significant for guiding the rational design and synthesis of novel, high-performance semiconductors.

2. RESULTS AND DISCUSSION

2.1. Synthesis and Characterization. The synthetic routes to the monomers and polymers (**PBDP-Fu**, **PBDP-Th**, and **PBDP-Se**) are outlined in Scheme 1. Briefly, the key BDP (**1**) core was synthesized in three steps starting from *p*-phenylenediamine, and the final oxidation step ensured conjugation of the quinodimethane structure (isolated yield of 60% over the three steps) according to the procedures established by Wudl et al.[19] A soluble BDP monomer was conveniently obtained by the subsequent alkylation of **2** with 2-decyltetradecyl bromide in anhydrous DMF in the presence of potassium carbonate, which was almost the same condition as that for other alkylated bislactom-based compounds (55% yield). All chalcogen-based counterpart distannylated comonomers (Fu, Th, and Se) were prepared using a lithiation and subsequent quenching with trimethyltin chloride.

Scheme 1. Synthetic Routes of BDP-Based Polymers[a]

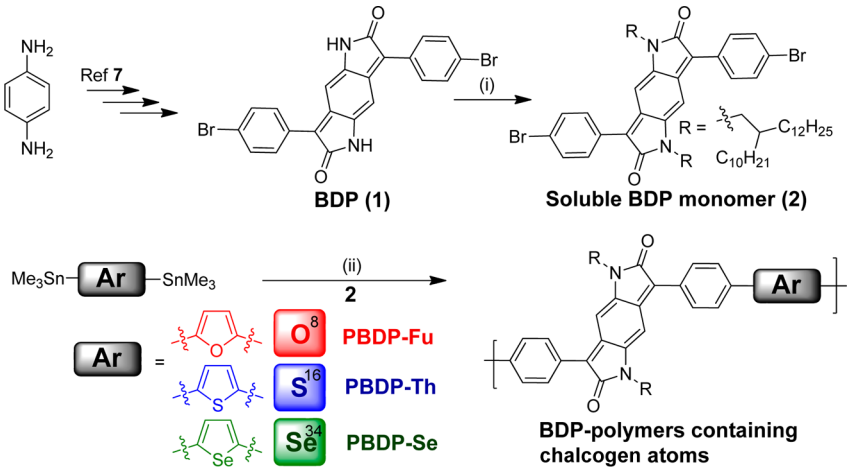

[a]Reagents and conditions: (i) K_2CO_3, DMF, 2-decyltetradecyl bromide 130 °C, 55%; (ii) $Pd(PPh_3)_4$, toluene, 110 °C, for **PBDP-Fu** (75%), **PBDP-Th** (70%), and **PBDP-Se** (81%).

dx.doi.org/10.1021/am405917a | ACS Appl. Mater. Interfaces 2014, 6, 4872−4882

Table 1. Photophysical and Electrochemical Properties of BDP-Based Polymers

polymer	M_n (kDa)	PDI	T_d (°C)[a]	λ_{max}^{sol} (nm)[b]	λ_{max}^{film} (nm)	E_g^{opt} (eV)[c]	E_{LUMO} (eV)[d]	E_{HOMO} (eV)[d]	E_g^{CV} (eV)[e]
PBDP-Fu	47.0	1.64	458	594	635	1.67	−3.60	−5.37	1.77
PBDP-Th	37.0	1.13	401	611	630	1.67	−3.58	−5.34	1.76
PBDP-Se	74.0	1.74	475	611	652	1.64	−3.59	−5.32	1.73

[a]The temperature of 5% weight-loss under nitrogen. [b]Chloroform solution. [c]Determined from the onset of the electronic absorption spectra. [d]Cyclic voltammetry determined with Fc/Fc+ (E_{HOMO} = −4.80 eV) as the internal reference. [e]E_g^{CV} = E_{LUMO} − E_{HOMO}.

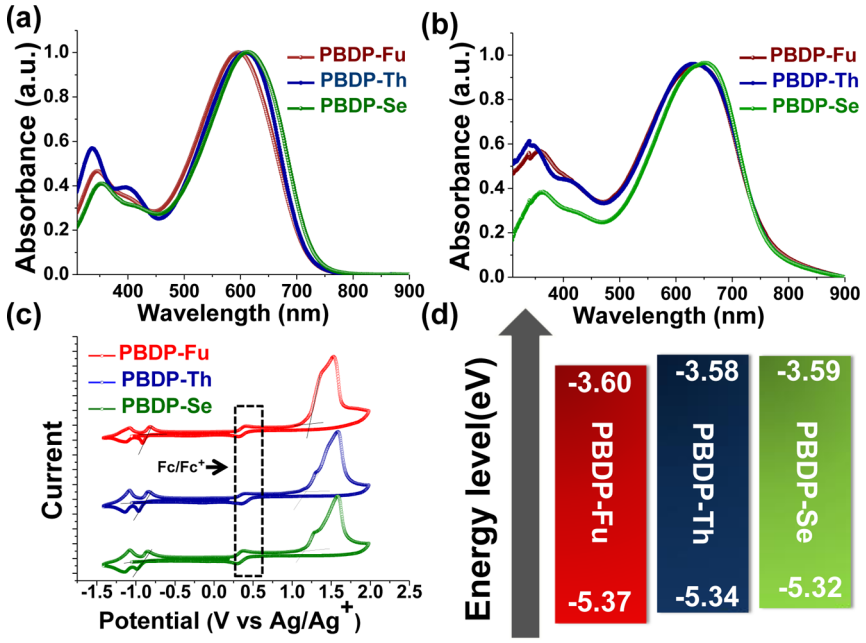

Figure 2. UV−vis absorption spectra of BDP-based polymers in chloroform solution (a) and as thin solid films (b). Cyclic voltammograms of BDP-based polymer thin films (c). Energy level diagrams for BDP-based polymers (d).

With all monomers in hand, the polymerizations were performed under a palladium (Pd)-catalyzed Stille-type coupling reaction, with 1:1 monomer ratio, to give the target polymers (see details in the Experimental section). This was followed by successive Soxhlet extraction with methanol, acetone, and hexane to remove catalyst residues and low molecular weight oligomers. The remaining material was dissolved in chloroform and precipitated into methanol, resulting in the pure target polymers, **PBDP-Fu**, **PBDP-Th**, and **PBDP-Se**. All of the polymers are highly soluble in organic solvents such as chloroform, THF, and chlorobenzene at room temperature. The number-average molecular weights (M_n) and the polydispersity index (PDI) of the polymers were determined by gel permeation chromatography (GPC) with THF as an eluent against polystyrene standards (Table 1). All polymerizations produced polymers with moderate to high molecular weights (37−74 kDa); the rather high molecular weight for **PBDP-Se** could be due to the aggregation that induced overestimation of molecular weight in THF. The thermal stability of all the polymers was also investigated by thermogravimetric analysis (TGA). **PBDP-Fu**, **PBDP-Th**, and **PBDP-Se** show a 5% weight loss at 458 °C, 401 °C, and 475 °C, respectively, which indicates their excellent thermal stability (see Table 1 and Figure S1 in the SI).

2.2. Photophysical and Electrochemical Properties and Computational Studies. The optical properties of the polymers were analyzed and are shown in Figure 2, with the detailed values listed in Table 1. All three polymers possess similar optical features with wide absorptions from 320 to 850 nm. Shorter and longer wavelength peaks are attributed to the $\pi-\pi^*$ transition band and intramolecular charge transfer (ICT) between donors and the acceptor BDP moiety, respectively. The absorption spectra of all the copolymer films show an obvious red-shift relative to their solutions, which is a general feature of D−A conjugated polymers because of their more ordered molecular organization in the solid films. It is worth noting that **PBDP-Se** exhibits an enhanced absorption intensity of the ICT band relative to that of the $\pi-\pi^*$ transition band, when compared to the strength ratios of the two peaks for **PBDP-Fu** and **PBDP-Th**.

Structurally, the three polymers differ from each other based on the identity of the donor conjugated with, and adjacent to, each BDP unit. Thereby, for **PBDP-Se**, the slight red-shift in the absorption maximum as well as the more pronounced ICT band imply the relatively stronger electron-donating ability of the Se than that of the other two moieties (Fu and Th). The optical bandgaps (E_g^{opt}), calculated from absorption cut off values, are determined as 1.67 eV, 1.67 eV, and 1.64 eV for **PBDP-Fu**, **PBDP-Th**, and **PBDP-Se** thin films, respectively.

It is relatively clear that organic semiconducting materials should have a delocalized electron-density-state and appropriate levels of the highest occupied molecular orbital (HOMO) and the lowest unoccupied molecular orbital (LUMO) to facilitate the efficient injection of the hole and electron from the electrode. Therefore, the electrochemical redox properties of the polymers were investigated as thin films using cyclic voltammetry (CV). The CV curves were recorded with reference to an Ag/Ag+ electrode and calibrated by the

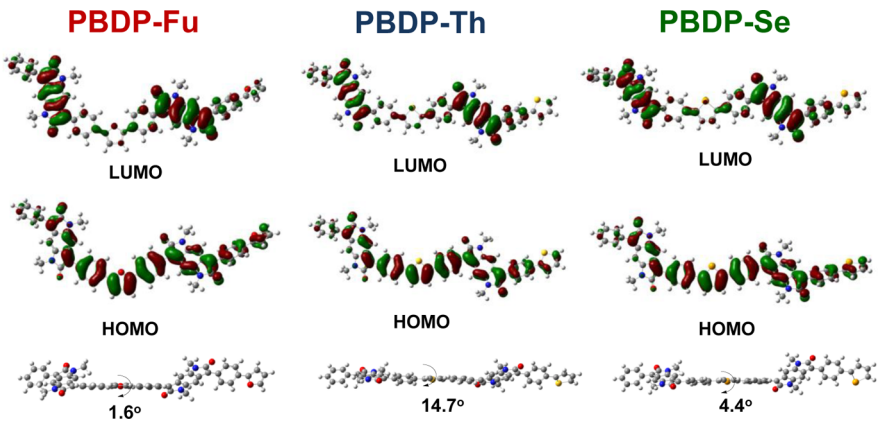

Figure 3. (a) DFT-optimized geometries and charge-density isosurfaces for the model dimers of BDP-based polymers (B3LYP/6-31G*) and their top views.

ferrocene/ferrocenium (Fc/Fc+) redox couple (absolute energy level of −4.80 eV to a vacuum) as an internal standard. These three polymers have two reversible redox processes at negative potential and quasi-reversible oxidation processes at a positive scan. Notably, these two characteristic BDP reduction waves not only indicate initial radical anion and subsequent dianion formation, but the reversibility in the reduction processes is also interpreted as a good sign of the stability of the BDP-polymer anions.

The oxidation and reduction onset potentials are translated to HOMO and LUMO energy levels, which are summarized in Table 1 and schematically depicted in Figure 2. Changing the donor parts (Fu, Th, and Se) of the BDP-based polymers barely affects the LUMO levels of the polymers (the three polymers with values between −3.58 and −3.60 eV), because their LUMOs are predominately localized on the strong accepting BDP core. On the other hand, the HOMOs relatively vary from −5.32 eV to −5.37 eV as a function of the electron donating ability of the donor monomer and polymer backbone conformation. This implies that the electron donating abilities of the donor chromophores increase in the order of Fu < Th < Se. The reasonably deep HOMO energy levels (below −5 eV) indicate good stability toward unintentional doping by atmospheric oxidants,[57] which is very important for manufacturing stable organic electronic devices. The electrochemical bandgaps defined as $E_g^{CV} = E_{LUMO} - E_{HOMO}$ for each polymer follow the same trends as the optical gaps but are consistently somewhat larger.

To gain insight into the structural and electronic features of the polymers, distributions of HOMO and LUMO of **PBDP-Fu**, **PBDP-Th**, and **PBDP-Se** were calculated using the DFT method at the B3LYP/6-31G* level and are shown in Figure 3. Interestingly, the HOMO is mostly distributed along the polymer backbone, whereas the LUMO is localized on the BDP moiety. This is consistent with the HOMO−LUMO distribution observed in several D−A polymers.[29,35,58−60] In addition, from the optimized structures of the polymers in the horizontal view, small dihedral angles of 1.6−14.7° between the BDP and chalcogen-based counits are observed, leading to the existence of good coplanarity in the main backbones.

2.3. Thin Film Microstructure Analyses. Conventional X-ray diffraction (XRD) and tapping-mode atomic force microscopy (AFM) analyses were carried out to investigate the thin film microstructures and morphologies on the substrate, which are the key factors that govern OFET device performance. Figure 4 exhibits XRD patterns of the annealed thin films of the BDP-based polymers, which enables us to specifically study the polymer chain alignment.

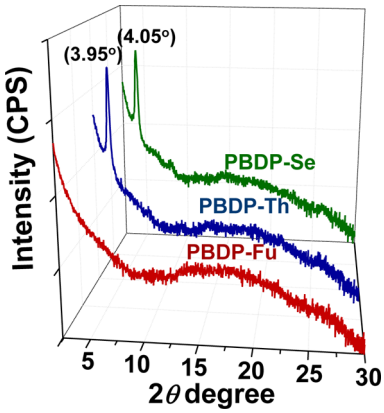

Figure 4. Out-of-plane X-ray diffraction (XRD) patterns of BDP-based polymer films annealed at 200 °C.

As shown in Figure 4, both **PBDP-Th** and **PBDP-Se** films show noticeable primary diffraction peaks with similar intensities at 2θ of 3.95° and 4.05°, corresponding to d(001)-spacing values of 22.36 and 21.82 Å, respectively, while no clear d(001)-diffraction peaks appeared in the films of **PBDP-Fu**. In addition, no observable π-stacking diffractions of polymer d(010) appeared in any of the cases. Judging from these XRD results, the films of **PBDP-Th** and **PBDP-Se** polymers preferentially adopt an edge-on orientation respective to the substrate, whereas **PBDP-Fu** are rather amorphous and exhibit no apparent surface structures, which is likely attributed to the less ordered intermolecular packing. In addition, as illustrated in Figure 5, compared to the **PBDP-Fu** film, both the **PBDP-Th** and **PBDP-Se** films have relatively denser grains. This visible change in the film crystallinity and morphology between **PBDP-Fu** and **PBDP-Th**/**PBDP-Se** likely stems from the stronger intermolecular interaction of **PBDP-Th**/**PBDP-Se** relative to **PBDP-Fu** films. This can be attributed to the larger overlap integrals and higher polarizabilities of sulfur and selenium (in Th and Se, respectively) compared to the lighter oxygen atom (in Fu).[44−46] Therefore, we would expect a facile charge transport in the **PBDP-Th** and **PBDP-Se** polymers, when compared to **PBDP-Fu** (*vide infra*).

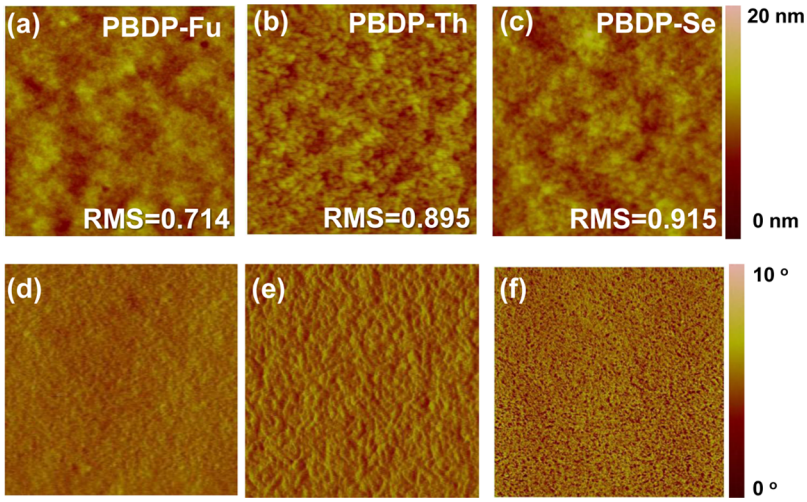

Figure 5. AFM height (top) and phase (bottom) images of (a, d) **PBDP-Fu**, (b, e) **PBDP-Th,** and (c, f) **PBDP-Se** films annealed at 200 °C.

2.4. OFETs Performance. Top gate, bottom contact OFETs with **PBDP-Th**, **PBDP-Se**, and **PBDP-Fu** were fabricated on a glass substrate with a poly(methyl methacrylate) (PMMA) gate dielectric layer. The conjugated polymer films are annealed at various temperatures from 100 to 250 °C for 30 min to improve device characteristics. Figure 6 shows the

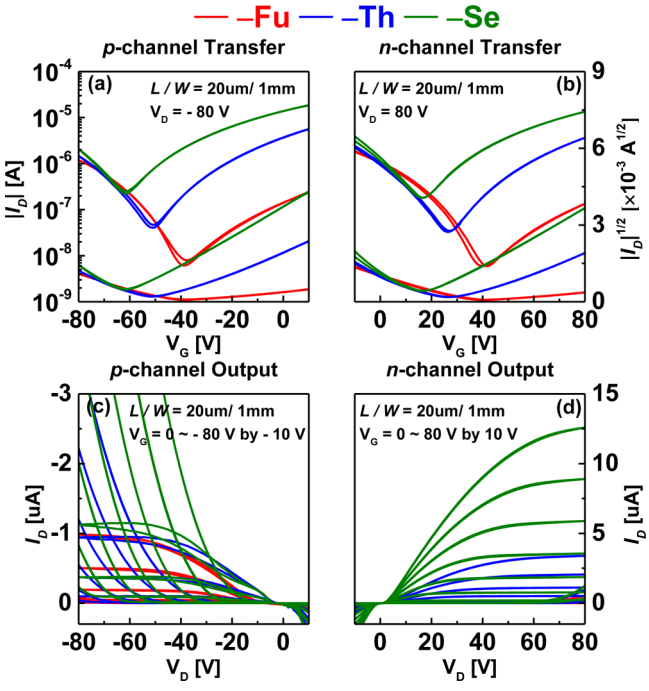

Figure 6. Transfer and output curve of 200 °C annealed **PBDP-Fu** (red line), **PBDP-Th** (blue line), and **PBDP-Se** (green line) OFETs. (a) *p*-channel and (b) *n*-channel transfer characteristics. (c) *p*-channel and (d) *n*-channel output characteristics.

typical transfer and output curves of the OFETs that were annealed at 200 °C; details of device properties including hole (μ_h) and electron mobility (μ_e) and threshold voltage (V_{TH}) are summarized in Table 2. All devices showed typical ambipolar OFETs characteristics with well-balanced μ_h and μ_e. The charge carrier mobilities of all devices are improved up to an order of magnitude by increasing the annealing temperature from 100 to 200 °C. This is mainly due to the improved crystallinity of polymer films by thermal annealing, which is observed in the XRD results (Figure 4, see the SI). A comparison between polymers revealed that **PBDP-Th** and **PBDP-Se** OFETs showed better μ_h and μ_e than **PBDP-Fu** OFETs due to a shorter intermolecular distance via a larger intermolecular interaction.[61] In addition, this result is consistent with our expectation based on XRD and AFM results. 200 °C annealed **PBDP-Se** OFETs showed the best and most well-balanced μ_h and μ_e of 1.7 × 10^{-2} cm^2/V·s and 1.9 cm × 10^{-2} cm^2/V·s, respectively. Even though the balance of μ_h and μ_e is one of the key factors to realize high performance complementary inverter based ICs and LETs, almost all 'push−pull' ambipolar conjugated polymers exhibited less balanced μ_h and μ_e since, not only do various parameters such as the crystallinity and orientation of the molecule, contact resistance, and quality of semiconductor-dielectric interface determine field-effect mobility in OFETs, but we cannot control the electron accepting and donating properties precisely via the design of the molecule. Therefore, the well balanced mobility in the BDP based copolymers here provides very useful information on how to design the D−A polymer to obtain well-balanced μ_h and μ_e.

To more clearly explain the sources of mobility difference in BDP polymers, contact resistance (R_c) and activation energy (E_A) for the electron and hole were measured using the Y-function method and low temperature I−V measurement, respectively. Details of the Y-function method have been described in our previous report and elsewhere.[62,63] As shown in Figure 7(a) and Table 3, a lower R_c was extracted from **PBDP-Th** and **PBDP-Se OFETs** than from the **PBDP-Fu** devices, and R_c of the electron and hole decreased by thermal annealing. This result indicates that a lower R_c in annealed devices is one of the reasons for the improvement of μ_h and μ_e by thermal annealing. The R_c for hole injection is almost similar for all polymers, whereas electron R_c shows a large difference as shown in Figure 7(b). This is an unexpected result since the three polymers have almost the same barrier height for electron and hole injection since all polymers have very similar LUMO and HOMO energetic levels. The larger electron R_c in **PBDP-Fu** OFETs is presumably due to the unfavorable molecular conformation, in particular the BDP unit, for efficient electron injection at the electrode-semiconductor interface.[64] E_A for electron and hole transport is extracted using Arrhenius

Table 2. Summary of the Electrical Characteristics of PBDP-Fu, PBDP-Th, and PBDP-Se OFETs Annealed at Various Temperatures[a]

		PBDP-Fu				PBDP-Th				PBDP-Se			
T_A		μ_{sat} [cm^2/V·s]	V_{TH} [V]	S.S [V/dec.]	I_{on}/I_{off}	μ_{sat} [cm^2/V·s]	V_{TH} [V]	S.S [V/dec.]	I_{on}/I_{off}	μ_{sat} [cm^2/V·s]	V_{TH} [V]	S.S [V/dec.]	I_{on}/I_{off}
100 °C	hole	5.0×10^{-4}	−28.6	−18.2	3×10^{-2}	4.5×10^{-3}	−47.4	−12.4	2×10^{-2}	7.2×10^{-3}	−52.0		1×10^{-1}
	electron	7.9×10^{-5}	17.5	33.1	1×10^{-1}	2.5×10^{-3}	35.7	19.9	1×10^{-2}	7.3×10^{-3}	11.0	16.0	2×10^{-2}
150 °C	hole	3.3×10^{-3}	−41.5	−12.0	8×10^{-3}	6.8×10^{-3}	−54.5	−11.8	2×10^{-2}	9.3×10^{-3}	−53.3	−20.2	1×10^{-1}
	electron	1.7×10^{-4}	34.5	25.0	9×10^{-2}	6.7×10^{-3}	35.5	13.9	7×10^{-3}	1.1×10^{-2}	16.8	17.7	2×10^{-2}
200 °C	hole	4.8×10^{-3}	−45.6	−10.4	6×10^{-3}	1.2×10^{-2}	−53.4	−14.5	3×10^{-2}	1.7×10^{-2}	−53.4	−18.5	1×10^{-1}
	electron	4.3×10^{-4}	40.2	18.7	5×10^{-2}	1.1×10^{-2}	34.2	17.2	5×10^{-3}	1.9×10^{-2}	19.1	19.8	2×10^{-2}
250 °C	hole	3.7×10^{-3}	−47.6	−12.3	2×10^{-2}	6.0×10^{-3}	−54.2	−15.2	8×10^{-2}	9.1×10^{-3}	−53.0	−18.1	1×10^{-1}
	electron	5.8×10^{-4}	27.5	20.7	4×10^{-2}	3.0×10^{-2}	30.4	10.6	4×10^{-3}	2.2×10^{-2}	19.9	14.1	9×10^{-3}

[a]All values are averaged from 6−9 devices.

plotting of μ_h and μ_e measured at a low temperature, and results are shown in Figure 8 and Table 4. The E_A follows similar trends to R_c. **PBDP-Se** and **PBDP-Th** OFETs showed lower electron and hole E_A than **PBDP-Fu**. Along with the R_c result, this is very consistent with the mobility trend of these devices and implies that the highest μ_h and μ_e in the **PBDP-Se** OFETs is mainly due to the lowest R_c and E_A, which is the result from the high crystallinity in XRD results in **PBDP-Se** and **PBDP-Th** films.

Finally, we demonstrated ambipolar complementary inverters using three conjugated polymers as a single active layer. Ambipolar conjugated polymers can transport both the electron and hole in one polymer chain so that the *p*- and *n*-channel semiconducting active regions in a complementary inverter can be formed by simple blanket coating such as spin coating and bar-coating without any patterning processes.[65] To achieve excellent inverter performance such as high voltage gain and a right inverting voltage at $V_{DD}/2$, high and well-balanced μ_h and μ_e ($V_{TH,h}$ and $V_{TH,e}$) are required. Figures 9(a) and 9(b) show the voltage transfer characteristics (VTCs) and the corresponding voltage gains of 200 °C annealed **PBDP-Fu**, **PBDP-Th**, and **PBDP-Se** ambipolar inverters at V_{DD} = 80 V. The V_{inv} of the complementary inverter is reached when both the *p*- and *n*-channel OFETs operate in the saturation region and can be expressed by eq 1

$$V_{inv} = \frac{V_{DD} + V_{Th}^{p} + V_{Th}^{n}\sqrt{\frac{\beta_n}{\beta_p}}}{1 + \sqrt{\frac{\beta_n}{\beta_p}}} \quad (1)$$

where $\beta = (W/L)\mu_{FET}C_i$ is a design factor for adjusting the *p*- and *n*-channel currents of the transistors, and the superscripts *p* and *n* denote the semiconductor type.[66] The V_{inv} of the **PBDP-Fu** device was the most theoretically ideal position at 1/2 V_{DD}, even though a large hysteresis was observed between the forward (V_{inv} = 57.4 V) and reverse (V_{inv} = 31.1 V) sweep due to the poorer device performances (Table 5) with the largest R_c (Table 5). On the other hand, **PBDP-Th** and **PBDP-Se** inverters showed a sharper inverting transition and a smaller hysteresis, but V_{inv} was shifted more to the left direction from 1/2 V_{DD} by ∼10 and 20 V, respectively. The right position of V_{inv} in the **PBDP-Fu** device was attributed to the more well-balanced $V_{TH,h}$ = −45.6 V and $V_{TH,e}$ = 40.1 V of the **PBDP-Fu** OFETs than those of the **PBDP-Th** ($V_{TH,h}$ = −53.4 V, $V_{TH,e}$ = 34.2 V) and **PBDP-Se** ($V_{TH,h}$ = −53.0 V, $V_{TH,e}$ = 19.1 V) inverters, since the position of V_{inv} mainly depends on the difference between the absolute value of $V_{TH,h}$ and $V_{TH,e}$. However, the **PBDP-Fu** devices showed the largest hysteresis in VTC because the device showed the largest R_c for electron and hole injection and lowest μ_h and μ_e. Even though the **PBDP-Se** devices showed the most shifted V_{inv}, the largest average inverter gain (∼20) was achieved in the **PBDP-Se** device compared with that of **PBDP-Th** (∼15) and **PBDP-Fu** (∼5). This is due to the highest and most well-balanced μ_h and μ_e in the **PBDP-Se** OFETs. From this study, we can control the inverter characteristics such as the VTCs and gains systematically by changing the molecular structure.

3. CONCLUSIONS

We designed and synthesized a family of three donor (D)−acceptor (A) polymer semiconductors (**PBDP-Fu**, **PBDP-Th**, and **PBDP-Se**) which polymerize donors of varying hetero-

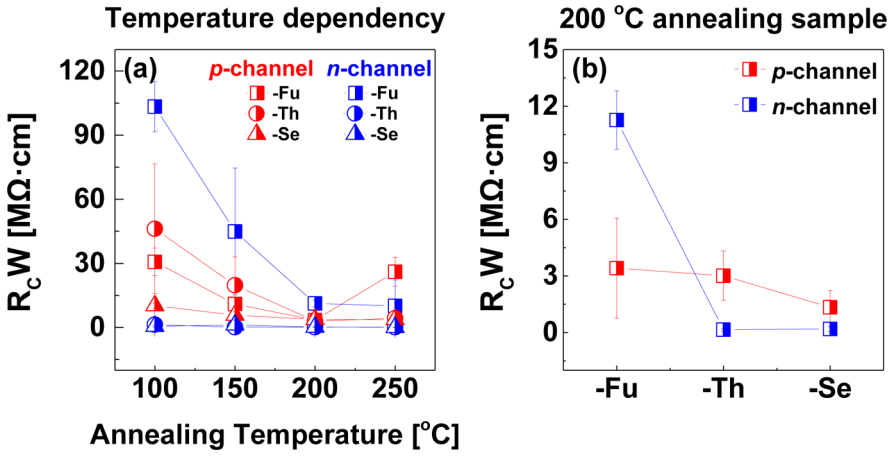

Figure 7. (a) Hole and electron contact resistance per unit channel width versus annealing temperature of **PBDP-Fu**, **PBDP-Th**, and **PBDP-Se** OFETs. (b) Hole and electron contact resistance of **PBDP-Fu**, **PBDP-Th**, and **PBDP-Se** OFETs annealed at 200 °C.

Table 3. Summary of Hole and Electron Contact Resistance for PBDP-Fu, PBDP-Th, and PBDP-Se OFETs Various Annealed Temperatures[a]

T_A		PBDP-Fu R_CW [MΩ·cm]	PBDP-Th R_CW [MΩ·cm]	PBDP-Se R_CW [MΩ·cm]
100 °C	hole	30.69 ± 6.48	46.20 ± 30.34	10.20 ± 1.26
	electron	103.31 ± 11.71	1.37 ± 1.64	0.58 ± 0.39
150 °C	hole	10.99 ± 7.64	19.76 ± 13.24	5.80 ± 1.65
	electron	44.87 ± 29.7	0.16 ± 0.09	1.20 ± 2.29
200 °C	hole	3.41 ± 2.65	3.01 ± 1.31	2.82 ± 3.99
	electron	11.26 ± 1.54	0.15 ± 0.07	0.13 ± 0.07
250 °C	hole	26.06 ± 6.75	4.32 ± 1.62	3.74 ± 1.38
	electron	10.13 ± 12.1	0.14 ± 0.21	0.05 ± 0.02

[a]All values are averaged from 6−9 devices.

aromatic blocks (furan (Fu), thiophene (Th), or selenophene (Se)) with the recently conceived benzodipyrrolidone (BDP) acceptor and that take on microstructural ordering with an edge-on configuration, whereas **PBDP-Fu** films take on an amorphous/low crystallinity alignment. Thereby, our confidence in both **PBDP-Th** and **PBDP-Se** as relatively higher performance polymers is justified by the aiming to systemically investigate the actual impact of the chalcogen atoms on intrinsic semiconducting properties. Given the similarity of the LUMO levels (−3.58 to −3.60 eV) due to the electron-accepting BDP moiety, the HOMO levels are shown to relatively depend on the donating companion units. XRD and AFM measurements reveal that both **PBDP-Th** and **PBDP-Se** polymer films with relatively heavier chalcogen atoms take on microstructural ordering with an edge-on configuration, whereas **PBDP-Fu** films take on a rather amorphous/low crystallinity alignment. Not only does **PBDP-Se** have both hole and electron mobilities exceeding 1.8 × 10^{-2} cm^2/V·s, but **PBDP-Th** also shows an almost equivalence between *p*-type operation and *n*-type operation, (μ_h = 1.2 × 10^{-2} cm^2/V·s) and (μ_e = 1.1 × 10^{-2} cm^2/V·s), respectively. Our studies provide generalizable insights into structure−property relationships on the existence of different heteroaromatic blocks in bislactam-based D−A polymers, which should facilitate the further design of high performance polymer semiconductors for OFETs.

4. EXPERIMENTAL SECTION

General Information. All reagents were purchased from Aldrich Co., Alfa Aesar, and TCI Co. and were used without purification. All solvents were used as fresh by distillation. Anhydrous THF was obtained by distillation from sodium/benzophenone prior to use. The intermediates based on benzodipyrrolidone (**1** and **2**)[19,20] as well as counterpart comonomers (2,5-bis(trimethylstannyl)furan,2,5-bis-(trimethylstannyl)thiophene, and 2,5-bis(trimethylstannyl)-selenophene))[67] were prepared according to the methods outlined in the literature. ^{1}H NMR and ^{13}C NMR spectra were recorded on an Agilent 400 MHz spectrophotometer using $CDCl_3$ as the solvent and tetramethylsilane (TMS) as the internal standard, and UV−vis-NIR spectra were taken on a UV-1800 (SHIMADZU) spectrometer. The

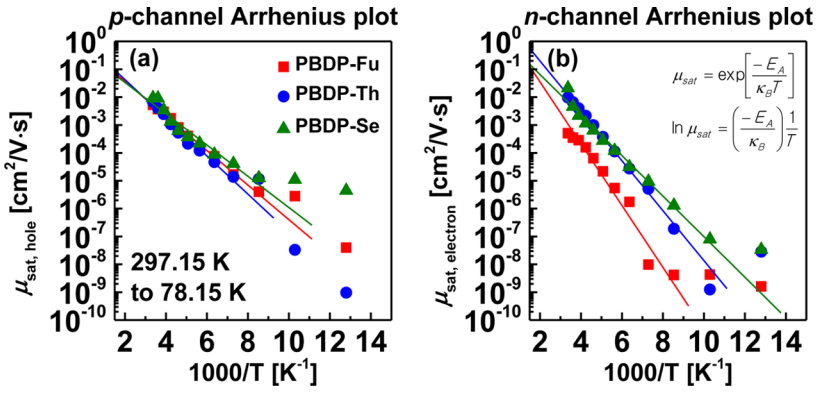

Figure 8. (a) Hole and (b) electron mobility (μ) versus 1000/temperature 200 °C annealed **PBDP-Fu**, **PBDP-Th**, and **PBDP-Se** OFETs. Devices were measured at various temperatures from 297.15 to 78.15 K at 20 K steps.

Table 4. Summary of Hole and Electron Activation Energy (E_A) of PBDP-Fu, PBDP-Th, and PBDP-Se OFETs

	hole		electron	
	$-E_A$ [meV] first region	$\mu_{sat,hole}$[cm^2/V·s] at 297.15 K	$-E_A$ [meV] first region	$\mu_{sat,electron}$ [cm^2/V·s] at 297.15 K
PBDP-Fu	−123	0.0052	−220.16	0.0006
PBDP-Th	−136	0.0068	−177.67	0.0097
PBDP-Se	−111	0.0093	−144.36	0.0212

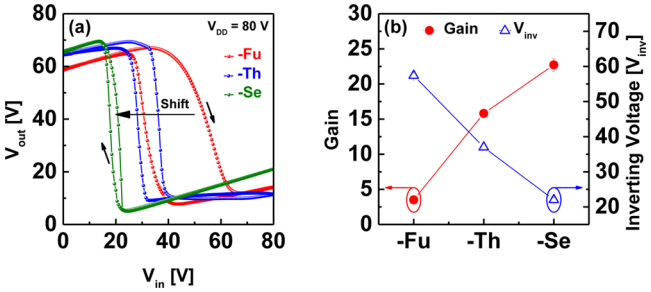

Figure 9. (a) Output characteristics of ambipolar complementary **PBDP-Fu**, **PBDP-Th**, and **PBDP-Se** inverters (W/L = 1000/20 μm for *n*- and *p*-channel transistors) and (b) gain and inverting voltage of complementary inverters annealed at 200 °C versus ambipolar polymers.

number-average (M_n) and weight average (M_w) molecular weights and the polydispersity index (PDI) of the polymer products were determined by gel permeation chromatography (GPC) with Perkin-Elmer Series 200 using a series of monodisperse polystyrene standards in THF (HPLC grade) at 313 K. Cyclic voltammetry (CV) measurements were performed on AMETEK VersaSTAT 3 with a three-electrode cell in a nitrogen bubbled 0.1 M tetra-*n*-butylammonium hexafluorophosphate (n-Bu_4NPF_6) solution in acetonitrile at a scan rate of 50 mV/s at room temperature. The CV was used as the Ag/Ag^+ (0.1 M of $AgNO_3$ in acetonitrile) reference electrode, platinum counter electrode, and polymer coated platinum working electrode, respectively. The Ag/Ag^+ reference electrode was calibrated using a ferrocene/ferrocenium redox couple as an internal standard, of which the oxidation potential is set at −4.8 eV with respect to a zero vacuum level.

General Procedure for Stille Polymerization and Polymer Purification. Compound (**2**) (0.13 mol) and distannyl compounds (0.13 mmol) were placed in a Schlenk tube under an argon atmosphere with 5 mL of anhydrous toluene. The mixture was degassed for 20 min followed by the addition of $Pd(PPh_3)_4$ (9.9 mol, 5 mol %). The mixture was heated at 110 °C for 24 h. After cooling to room temperature, the mixture was poured into methanol, and the resulting precipitate was filtered. The polymer was purified by Soxhlet extraction using methanol, acetone, and hexane and finally extracted with chloroform. The chloroform solution was then concentrated by evaporation and reprecipitated in methanol. The resulting dark blue colored solids were collected and dried overnight under vacuum. The polymers were characterized by ^{1}H NMR, GPC, and elemental analysis.

PBDP-Fu. Isolated yield = 75%. M_n = 47.0 kDa, M_w = 82.0 kDa, and PDI = 1.74 (against PS standard), ^{1}H NMR ($CDCl_3$,400 MHz): δ ppm 7.78−7.92 (br 8H), 6.85 (s, 2H), 6.43 (s, 2H), 3.56 (s, 4H), 1.82 (br, 4H), 1.38 (br 8H), 1.20−1.43 (br, 70H), 0.84−0.92 (br, 12H). Anal. Calcd. for $C_{74}H_{110}N_2O_3$: C, 82.63; H, 10.31; N, 2.60; O, 4.46; found: C, 82.53; H, 10.47; N, 2.38.

PBDP-Th. Isolated yield = 70%. M_n = 37.0 kDa, M_w = 61.0 kDa, PDI = 1.64 (against PS standard), ^{1}H NMR ($CDCl_3$, 400 MHz) δ ppm 7.75−7.78 (br, 4H), 7.30−7.73 (br, 4H), 6.20−6.42 (br, 4H), 3.54 (br, 4H), 1.80 (br, 2H), 1.65 (br, 10H), 1.22−1.40 (br, 70H), 0.83−0.91 (br, 12H). Anal. Calcd. for $C_{74}H_{110}N_2O_2S$ C, 81.41; H, 10.16; N, 2.57; O, 2.93; S, 2.94; found: C, 81.54; H, 10.19; N, 2.78; S, 3.10.

PBDP-Se. Isolated yield = 81%. M_n = 74.0 kDa, M_w = 84.0 kDa, PDI = 1.13 (against PS standard), ^{1}H NMR ($CDCl_3$, 400 MHz): δ ppm 7.59−7.78 (br, 8H), 7.39−7.57 (br, 2H), 6.42 (s, 2H), 3.47−3.54 (br, 4H), 1.80 (br, 2H), 1.65 (br, 10H), 1.22−1.40 (br, 70H), 0.83−0.91 (br, 12H). Anal. Calcd. for $C_{74}H_{110}N_2O_2Se$: C, 78.06; H, 9.74; N, 2.46; O, 2.81; Se, 6.93; found: C, 78.23; H, 9.78; N, 2.36.

OFETs and Complementary Inverters Fabrication. Cr/Au (2 nm/13 nm) source/drain patterns were performed on Corning Eagle XG glass substrates using a conventional lift-off photolithography process with positive-tone photoresist and thermal evaporation. Before use, the substrates were cleaned sequentially in a sonication bath of acetone, isopropanol, and deionized water for 10 min each. Ambipolar **PBDP-X** copolymer was synthesized and used without any further purification. This semiconductor was dissolved in anhydrous chlorobenzene (Sigma Aldrich) to obtain 8 mg/mL solution and was spin coated at 1400 rpm for 90 s and then thermally annealed at temperatures ranging from 100 to 250 °C for 30 min in an N_2-purged glovebox. 80 mg/mL of PMMA (Sigma Aldrich, ~120 kM_w) in an nBA concentrate solution was used as the gate-dielectric and was spin-coated at 2000 rpm for 60 s and then baked at 80 °C for 1 h (thickness ~500 nm, capacitance: 6.20 nF/cm^2) in an N_2-purged glovebox. The transistors were completed by depositing the top gate electrodes (Al) via thermal evaporation using a metal shadow mask. For the complementary inverters, circuit electrodes were patterned using photolithography, as above. In addition, the semiconductor and gate dielectric layers were deposited by a simple spin coating process. Complementary inverters were completed by deposition of the top gate electrodes on the active regions of the *n*- and *p*-channel transistors.

Characterization. The electrical characteristics of the OFETs were extracted from the drain current via gate voltage bias or drain voltage bias (channel width (W)/length (L): 1000/20 μm). The channel width and length of *n*- and *p*-channel transistors in the complementary inverters are 1000 and 20 μm, respectively. Activation energy was extracted from the mobility via a vacuum state probe chamber while decreasing the temperature from 297.15 to 78.15 K in 20 K steps using liquid nitrogen. All measurements were taken using a Keithley 4200-SCS semiconductor parameter analyzer connected to an N_2-purged glovebox probe station.

Table 5. Summary of Gain and Inverting Voltage (V_{inv}) for PBDP-Fu, PBDP-Th, and PBDP-Se Complementary Inverters

	PBDP-Fu			PBDP-Th			PBDP-Se		
	gain	V_{inv}	$\Delta V_{TH,m}$	gain	V_{inv}	$\Delta V_{TH,m}$	gain	V_{inv}	$\Delta V_{TH,m}$
forward	3.50	57.40	−2.72	15.81	37.00	−9.59	22.72	22.00	−17.18
reverse	8.61	31.10		14.33	28.00		18.73	17.20	

dx.doi.org/10.1021/am405917a | ACS Appl. Mater. Interfaces 2014, 6, 4872−4882

■ ASSOCIATED CONTENT

Supporting Information

TGA data of **PBDP-Fu**, **PBDP-Th**, and **PBDP-Se** and XRD data at R.T. This material is available free of charge via the Internet at http://pubs.acs.org.

■ AUTHOR INFORMATION

Corresponding Authors

*E-mail: yynoh@dongguk.edu.
*E-mail: yang@unist.ac.kr.

Author Contributions

§These authors contributed equally.

Notes

The authors declare no competing financial interest.

■ ACKNOWLEDGMENTS

This research was supported by the Basic Science Research Program through the National Research Foundation of Korea (NRF) funded by the Ministry of Science, ICT and Future Planning (Grant No.: 2013R1A1A1A05004475, 2010-0019408, BK21 Plus (10Z20130011057)). This research was also supported by the International Cooperation of the Korea Institute of Energy Technology Evaluation and Planning (KETEP) grant funded by the Korea government Ministry of Knowledge Economy (20123010010140), by a grant from the Centre for Advanced Soft Electronics under the Global Frontier Research Program of the Ministry of Science, ICT and Future Planning (code no. 2013M3A6A5073183) and by the Dongguk University Research Fund of 2013.

■ REFERENCES

(1) Baeg, K.-J.; Caironi, M.; Noh, Y.-Y. Toward Printed Integrated Circuits based on Unipolar or Ambipolar Polymer Semiconductors. *Adv. Mater.* **2013**, *25*, 4210−4244.

(2) Schenning, A. P.; Meijer, E. Supramolecular Electronics; Nanowires from Self-assembled π-Conjugated Systems. *Chem. Commun.* **2005**, *26*, 3245−3258.

(3) Barbara, P. F.; Gesquiere, A. J.; Park, S.-J.; Lee, Y. J. Single-Molecule Spectroscopy of Conjugated Polymers. *Acc. Chem. Res.* **2005**, *38*, 602−610.

(4) Tao, N. Electron Transport in Molecular Junctions. *Nat. Nanotechnol.* **2006**, *1*, 173−181.

(5) Taniguchi, M.; Nojima, Y.; Yokota, K.; Terao, J.; Sato, K.; Kambe, N.; Kawai, T. Self-Organized Interconnect Method for Molecular Devices. *J. Am. Chem. Soc.* **2006**, *128*, 15062−15063.

(6) Lafferentz, L.; Ample, F.; Yu, H.; Hecht, S.; Joachim, C.; Grill, L. Conductance of a Single Conjugated Polymer as a Continuous Function of Its Length. *Science* **2009**, *323*, 1193−1197.

(7) Chen, X.; Braunschweig, A. B.; Wiester, M. J.; Yeganeh, S.; Ratner, M. A.; Mirkin, C. A. Spectroscopic Tracking of Molecular Transport Junctions Generated by Using Click Chemistry. *Angew. Chem., Int. Ed.* **2009**, *48*, 5178−5181.

(8) Joachim, C.; Gimzewski, J.; Aviram, A. Electronics Using Hybrid-Molecular and Mono-Molecular Devices. *Nature* **2000**, *408*, 541−548.

(9) Li, J.; Zhao, Y.; Tan, H. S.; Guo, Y.; Di, C.-A.; Yu, G.; Liu, Y.; Lin, M.; Lim, S. H.; Zhou, Y. A Stable Solution-Processed Polymer Semiconductor with Record High-Mobility for Printed Transistors. *Sci. Rep.* **2012**, *2*, 754.

(10) Baeg, K.-J.; Khim, D.; Jung, S. W.; Kang, M.; You, I. K.; Kim, D. Y.; Facchetti, A.; Noh, Y.-Y. Remarkable Enhancement of Hole Transport in Top-Gated *n*-Type Polymer Field-Effect Transistors by a High-k Dielectric for Ambipolar Electronic Circuits. *Adv. Mater.* **2012**, *24*, 5433−5439.

(11) Zaumseil, J.; Friend, R. H.; Sirringhaus, H. Spatial Control of the Recombination Zone in an Ambipolar Light-Emitting Organic Transistor. *Nat. Mater.* **2005**, *5*, 69−74.

(12) Baeg, K.-J.; Kim, J.; Khim, D.; Caironi, M.; Kim, D.-Y.; You, I.-K.; Quinn, J. R.; Facchetti, A.; Noh, Y.-Y. Charge Injection Engineering of Ambipolar Field-Effect Transistors for High-Performance Organic Complementary Circuits. *ACS Appl. Mater. Interfaces* **2011**, *3*, 3205−3214.

(13) Qu, S.; Tian, H. Diketopyrrolopyrrole (DPP)-Based Materials for Organic Photovoltaics. *Chem. Commun.* **2012**, *48*, 3039−3051.

(14) Lee, J.; Han, A.; Hong, J.; Seo, J. H.; Oh, J. H.; Yang, C. Inversion of Dominant Polarity in Ambipolar Polydiketopyrrolopyrrole with Thermally Removable Groups. *Adv. Funct. Mater.* **2012**, *22*, 4128−4138.

(15) Lee, J.; Cho, S.; Seo, J. H.; Anant, P.; Jacob, J.; Yang, C. Swapping Field-Effect Transistor Characteristics in Polymeric Diketopyrrolopyrrole Semiconductors: Debut of an Electron Dominant Transporting Polymer. *J. Mater. Chem.* **2012**, *22*, 1504−1510.

(16) Lee, J.; Cho, S.; Yang, C. Highly Reproducible Organic Field-Effect Transistor from Pseudo 3-Dimensional Triphenylamine-Based Amorphous Conjugated Copolymer. *J. Mater. Chem.* **2011**, *21*, 8528−8531.

(17) Lee, J.; Yun, M. H.; Kim, J.; Kim, J. Y.; Yang, C. Toward the Realization of A Practical Diketopyrrolopyrrole-Based Small Molecule for Improved Efficiency in Ternary BHJ Solar Cells. *Macromol. Rapid Commun.* **2012**, *33*, 140−145.

(18) Cho, S.; Lee, J.; Tong, M.; Seo, J. H.; Yang, C. Poly(diketopyrrolopyrrole-benzothiadiazole) with Ambipolarity Approaching 100% Equivalency. *Adv. Funct. Mater.* **2011**, *21*, 1910−1916.

(19) Cui, W.; Yuen, J.; Wudl, F. Benzodipyrrolidones and Their Polymers. *Macromolecules* **2011**, *44*, 7869−7873.

(20) Hong, W.; Guo, C.; Li, Y.; Zheng, Y.; Huang, C.; Lu, S.; Facchetti, A. Synthesis and Thin-Film Transistor Performance of Benzodipyrrolinone and Bithiophene Donor-Acceptor Copolymers. *J. Mater. Chem.* **2012**, *22*, 22282−22289.

(21) Yue, W.; Huang, X.; Yuan, J.; Ma, W.; Krebs, F. C.; Yu, D. A Novel Benzodipyrrolidone-Based Low Bandgap Polymer for Organic Solar Cells. *J. Mater. Chem. A* **2013**, *1*, 10116−10119.

(22) Deng, P.; Liu, L.; Ren, S.; Li, H.; Zhang, Q. *N*-Acylation: An Effective Method for Reducing the LUMO Energy Levels of Conjugated Polymers Containing Five-Membered Lactam Units. *Chem. Commun.* **2012**, *48*, 6960−6962.

(23) Stalder, R.; Mei, J.; Reynolds, J. R. Isoindigo-Based Donor−Acceptor Conjugated Polymers. *Macromolecules* **2010**, *43*, 8348−8352.

(24) Zhang, G.; Fu, Y.; Xie, Z.; Zhang, Q. Synthesis and Photovoltaic Properties of New Low Bandgap Isoindigo-Based Conjugated Polymers. *Macromolecules* **2011**, *44*, 1414−1420.

(25) Stalder, R.; Mei, J.; Subbiah, J.; Grand, C.; Estrada, L. A.; So, F.; Reynolds, J. R. *n*-Type Conjugated Polyisoindigos. *Macromolecules* **2011**, *44*, 6303−6310.

(26) Lei, T.; Dou, J.-H.; Ma, Z.-J.; Yao, C.-H.; Liu, C.-J.; Wang, J.-Y.; Pei, J. Ambipolar Polymer Field-Effect Transistors Based on Fluorinated Isoindigo: High Performance and Improved Ambient Stability. *J. Am. Chem. Soc.* **2012**, *134*, 20025−20028.

(27) Stalder, R.; Grand, C.; Subbiah, J.; So, F.; Reynolds, J. R. An Isoindigo and Dithieno [3,2-*b*:2′,3′-*d*] silole Copolymer for Polymer Solar Cells. *Polym. Chem.* **2012**, *3*, 89−92.

(28) Wang, E.; Ma, Z.; Zhang, Z.; Vandewal, K.; Henriksson, P.; Inganäs, O.; Zhang, F.; Andersson, M. R. An Easily Accessible Isoindigo-Based Polymer for High-Performance Polymer Solar Cells. *J. Am. Chem. Soc.* **2011**, *133*, 14244−14247.

(29) Dutta, G. K.; Han, A.; Lee, J.; Kim, Y.; Oh, J. H.; Yang, C. Visible-Near Infrared Absorbing Polymers Containing Thienoisoindigo and Electron-Rich Units for Organic Transistors with Tunable Polarity. *Adv. Funct. Mater.* **2013**, *23*, 5317−5325.

(30) Koizumi, Y.; Ide, M.; Saeki, A.; Vijayakumar, C.; Balan, B.; Kawamoto, M.; Seki, S. Thienoisoindigo-Based Low-Bandgap Polymers for Organic Electronic Devices. *Polym. Chem.* **2013**, *4*, 484−494.

(31) Van Pruissen, G. W.; Gholamrezaie, F.; Wienk, M. M.; Janssen, R. A. Synthesis and Properties of Small Band Gap Thienoisoindigo Based Conjugated Polymers. *J. Mater. Chem.* **2012**, *22*, 20387−20393.
(32) Ashraf, R. S.; Kronemeijer, A. J.; James, D. I.; Sirringhaus, H.; McCulloch, I. A New Thiophene Substituted Isoindigo Based Copolymer for High performance Ambipolar Transistors. *Chem. Commun.* **2012**, *48*, 3939−3941.
(33) Mei, J.; Graham, K. R.; Stalder, R.; Reynolds, J. R. Synthesis of Isoindigo-Based Oligothiophenes for Molecular Bulk Heterojunction Solar Cells. *Org. Lett.* **2010**, *12*, 660−663.
(34) Mei, J.; Kim, D. H.; Ayzner, A. L.; Toney, M. F.; Bao, Z. Siloxane-Terminated Solubilizing Side Chains: Bringing Conjugated Polymer Backbones Closer and Boosting Hole Mobilities in Thin-Film Transistors. *J. Am. Chem. Soc.* **2011**, *133*, 20130−20133.
(35) Lee, J.; Han, A.-R.; Yu, H.; Shin, T. J.; Yang, C.; Oh, J. H. Boosting the Ambipolar Performance of Solution-Processable Polymer Semiconductors via Hybrid Side-Chain Engineering. *J. Am. Chem. Soc.* **2013**, *135*, 9540−9547.
(36) Lee, J.; Han, A.-R.; Kim, J.; Kim, Y.; Oh, J. H.; Yang, C. Solution-Processable Ambipolar Diketopyrrolopyrrole-Selenophene Polymer with Unprecedentedly High Hole and Electron Mobilities. *J. Am. Chem. Soc.* **2012**, *134*, 20713−20721.
(37) Shahid, M.; McCarthy-Ward, T.; Labram, J.; Rossbauer, S.; Domingo, E. B.; Watkins, S. E.; Stingelin, N.; Anthopoulos, T. D.; Heeney, M. Low Bandgap Selenophene-Diketopyrrolopyrrole Polymers Exhibiting High and Balanced Ambipolar Performance in Bottom-Gate Transistors. *Chem. Sci.* **2012**, *3*, 181−185.
(38) Kronemeijer, A. J.; Gili, E.; Shahid, M.; Rivnay, J.; Salleo, A.; Heeney, M.; Sirringhaus, H. A Selenophene-Based Low-Bandgap Donor-Acceptor Polymer Leading to Fast Ambipolar Logic. *Adv. Mater.* **2012**, *24*, 1558−1565.
(39) Ha, J. S.; Kim, K. H.; Choi, D. H. 2,5-Bis(2-octyldodecyl)-pyrrolo[3,4-*c*]pyrrole-1,4-(2*H*,5*H*)-dione-Based Donor-Acceptor Alternating Copolymer Bearing 5,5′-Di(thiophen-2-yl)-2, 2′-biselenophene Exhibiting 1.5 $cm^2 \cdot V^{-1} \cdot s^{-1}$ Hole Mobility in Thin-Film Transistors. *J. Am. Chem. Soc.* **2011**, *133*, 10364−10367.
(40) Gidron, O.; Dadvand, A.; Sheynin, Y.; Bendikov, M.; Perepichka, D. F. Towards "Green" Electronic Materials. α-Oligofurans as Semiconductors. *Chem. Commun.* **2011**, *47*, 1976−1978.
(41) Woo, C. H.; Beaujuge, P. M.; Holcombe, T. W.; Lee, O. P.; Fréchet, J. M. Incorporation of Furan Into Low Band-Gap Polymers for Efficient Solar Cells. *J. Am. Chem. Soc.* **2010**, *132*, 15547−15549.
(42) Bunz, U. H. α-Oligofurans: Molecules without a Twist. *Angew. Chem., Int. Ed.* **2010**, *49*, 5037−5040.
(43) Chen, Z.; Wannere, C. S.; Corminboeuf, C.; Puchta, R.; Schleyer, P. v. R. Nucleus-Independent Chemical Shifts (NICS) as an Aromaticity Criterion. *Chem. Rev.* **2005**, *105*, 3842−3888.
(44) Takimiya, K.; Kunugi, Y.; Konda, Y.; Niihara, N.; Otsubo, T. 2,6-Diphenylbenzo[1,2-*b*:4,5-*b*']dichalcogenophenes: A New Class of High-Performance Semiconductors for Organic Field-Effect Transistors. *J. Am. Chem. Soc.* **2004**, *126*, 5084−5085.
(45) Hutchison, G. R.; Ratner, M. A.; Marks, T. J. Intermolecular Charge Transfer between Heterocyclic Oligomers. Effects of Heteroatom and Molecular Packing on Hopping Transport in Oganic Smiconductors. *J. Am. Chem. Soc.* **2005**, *127*, 16866−16881.
(46) Sharma, S.; Bendikov, M. α-Oligofurans: A Computational Study. *Chem.—Eur. J.* **2013**, *19*, 13127−13139.
(47) Bijleveld, J. C.; Karsten, B. P.; Mathijssen, S. G.; Wienk, M. M.; de Leeuw, D. M.; Janssen, R. A. Small Band Gap Copolymers Based on Furan and Diketopyrrolopyrrole for Field-Effect Transistors and Photovoltaic Cells. *J. Mater. Chem.* **2011**, *21*, 1600−1606.
(48) Yuan, J.; Huang, X.; Zhang, F.; Lu, J.; Zhai, Z.; Di, C.; Jiang, Z.; Ma, W. Design of Benzodithiophene-Diketopyrrolopyrrole Based Donor-Acceptor Copolymers for Efficient Organic Field Effect Transistors and Polymer Solar Cells. *J. Mater. Chem.* **2012**, *22*, 22734−22742.
(49) Yuan, J.; Zang, Y.; Dong, H.; Liu, G.; Di, C.; Li, Y.; Ma, W. Effect of Furan π-Bridge on Polymer Coplanarity and Performance in Organic Field Effect Transistors. *Polym. Chem.* **2013**, *4*, 4199−4260.
(50) Sonar, P.; Foong, T. R. B.; Singh, S. P.; Li, Y.; Dodabalapur, A. A Furan-Containing Conjugated Polymer for High Mobility Ambipolar Organic Thin Film Transistors. *Chem. Commun.* **2012**, *48*, 8383−8385.
(51) Li, Y.; Sonar, P.; Murphy, L.; Hong, W. High Mobility Diketopyrrolopyrrole (DPP)-Based Organic Semiconductor Materials for Organic Thin Film Transistors and Photovoltaics. *Energy Environ. Sci.* **2013**, *6*, 1684−1710.
(52) Li, Y.; Sonar, P.; Singh, S. P.; Zeng, W.; Soh, M. S. 3,6-Di(furan-2-yl)pyrrolo[3,4-*c*] pyrrole-1,4(2*H*,5*H*)-dione and Bithiophene Copolymer with Rather Disordered Chain Orientation Showing High Mobility in Organic Thin Film transistors. *J. Mater. Chem.* **2011**, *21*, 10829−10835.
(53) Li, Y.; Sonar, P.; Singh, S. P.; Soh, M. S.; van Meurs, M.; Tan, J. Annealing-Free High-Mobility Diketopyrrolopyrrole-Quaterthiophene Copolymer for Solution-Processed Organic Thin Film Transistors. *J. Am. Chem. Soc.* **2011**, *133*, 2198−2204.
(54) Dou, L.; Chang, W. H.; Gao, J.; Chen, C. C.; You, J.; Yang, Y. A Selenium-Substituted Low-Bandgap Polymer with Versatile Photovoltaic Applications. *Adv. Mater.* **2013**, *25*, 825−831.
(55) Pati, P. B.; Senanayak, S. P.; Narayan, K.; Zade, S. S. Solution Processable Benzooxadiazole and Benzothiadiazole Based DAD Molecules with Chalcogenophene: Field Effect Transistor Study and Structure Property Relationship. *ACS Appl. Mater. Interfaces* **2013**, *5*, 12460−12468.
(56) Nakano, M.; Mori, H.; Shinamura, S.; Takimiya, K. Naphtho-[2,3-*b*:6,7-*b*'] dichalcogenophenes: Syntheses, Characterizations, and Chalcogene Atom Effects on Organic Field-Effect Transistor and Organic Photovoltaic Devices. *Chem. Mater.* **2011**, *24*, 190−198.
(57) Rumer, J. W.; Levick, M.; Dai, S.-Y.; Rossbauer, S.; Huang, Z.; Biniek, L.; Anthopoulos, T. D.; Durrant, J.; Procter, D. J.; McCulloch, I. BPTs: Thiophene-Flanked Benzodipyrrolidone Conjugated Polymers for Ambipolar Organic Transistors. *Chem. Commun.* **2013**, *49*, 4465−4467.
(58) Kim, Y.; Hong, J.; Oh, J. H.; Yang, C. Naphthalene Diimide Incorporated Thiophene-Free Copolymers with Acene and Heteroacene Units: Comparison of Geometric Features and Electron-Donating Strength of Co-units. *Chem. Mater.* **2013**, *25*, 3251−3259.
(59) Kim, Y.; Yeom, H. R.; Kim, J. Y.; Yang, C. High-Efficiency Polymer Solar Cells with a Cost-Effective Quinoxaline Polymer Through Nanoscale Morphology Control Induced by Practical Processing Additives. *Energy Environ. Sci.* **2013**, *6*, 1909−1916.
(60) Kim, B.; Yeom, H. R.; Yun, M. H.; Kim, J. Y.; Yang, C. A Selenophene Analogue of PCDTBT: Selective Fine-Tuning of LUMO to Lower of the Bandgap for Efficient Polymer Solar Cells. *Macromolecules* **2012**, *45*, 8658−8664.
(61) Kang, I.; An, T. K.; Hong, J.; Yun, H. J.; Kim, R.; Chung, D. S.; Park, C. E.; Kim, Y. H.; Kwon, S. K. Effect of Selenophene in a DPP Copolymer Incorporating a Vinyl Group for High-Performance Organic Field-Effect Transistors. *Adv. Mater.* **2013**, *25*, 524−528.
(62) Baeg, K.-J.; Bae, G.-T.; Noh, Y.-Y. Efficient Charge Injection in *p*-Type Polymer Field-Effect Transistors with Low-Cost Molybdenum Electrodes through V_2O_5 Interlayer. *ACS Appl. Mater. Interfaces* **2013**, *5*, 5804−5810.
(63) Xu, Y.; Minari, T.; Tsukagoshi, K.; Chroboczek, J.; Ghibaudo, G. Direct Evaluation of Low-Field Mobility and Access Resistance in Pentacene Field-Effect Transistors. *J. Appl. Phys.* **2010**, *107*, 114507−114507−7.
(64) Fabiano, S.; Yoshida, H.; Chen, Z.; Facchetti, A.; Loi, M. A. Orientation-Dependent Electronic Structures and Charge Transport Mechanisms in Ultra-Thin Polymeric *n*-Channel Field-Effect Transistors. *ACS Appl. Mater. Interfaces* **2013**, *5*, 4417−4422.
(65) Khim, D.; Han, H.; Baeg, K. J.; Kim, J.; Kwak, S. W.; Kim, D. Y.; Noh, Y.-Y. Simple Bar-Coating Process for Large-Area, High-Performance Organic Field-Effect Transistors and Ambipolar Complementary Integrated Circuits. *Adv. Mater.* **2013**, *25*, 4302−4308.

(66) Rabaey, J.; Chandrakasan, A.; Nikolic, B. *Digital Integrated Circuits (Printice-Hall Electronics and VLSI series)*; Prentice-Hall: Englewood Cliffs, NJ, 2003.
(67) Lei, T.; Cao, Y.; Zhou, X.; Peng, Y.; Bian, J.; Pei, J. Systematic Investigation of Isoindigo-Based Polymeric Field-Effect Transistors: Design Strategy and Impact of Polymer Symmetry and Backbone Curvature. *Chem. Mater.* **2012**, *24*, 1762−1770.